

# High-brilliance ultra-narrow-band x-rays via electron radiation in colliding laser pulses

Q. Z. Lv,<sup>1,\*</sup> E. Raicher,<sup>2,†</sup> C. H. Keitel,<sup>1</sup> and K. Z. Hatsagortsyan<sup>1</sup>

<sup>1</sup>Max-Planck-Institut für Kernphysik, Saupfercheckweg 1, 69117 Heidelberg, Germany

<sup>2</sup>Soreq Nuclear Research Center, 81800 Yavne, Israel

(Dated: January 19, 2022)

A setup of a unique x-ray source is put forward employing a relativistic electron beam interacting with two counter-propagating laser pulses in the nonlinear few-photon regime. In contrast to Compton scattering sources, the envisaged x-ray source exhibits an extremely narrow relative bandwidth of the order of  $10^{-4}$ , comparable with an x-ray free-electron laser (XFEL). The brilliance of the x-rays can be an order of magnitude higher than that of a state-of-the-art Compton source. By tuning the laser intensities and the electron energy, one can realize either a single peak or a comb-like x-ray source of around keV energy. The laser intensity and the electron energy in the suggested setup are rather moderate, rendering this scheme compact and table-top size, as opposed to XFEL and synchrotron infrastructures.

Ever since the discovery by W. C. Röntgen in 1895, powerful x-ray techniques have been developed for determining the structure of matter at the atomic length scale [1, 2]. Remarkable advancements have been achieved with the employment of synchrotron radiation [3–6], and the x-ray free-electron laser (XFEL) [7–12], which dramatically increased the brightness of the source. Unfortunately, the large size and cost of these facilities, limit their accessibility to a wide community. Alternative schemes rely on Thomson- and Compton-scattering (CS) [13–16], and recently also on the radiation from laser-plasma interactions [17–20]. The advancement of compact and powerful laser systems revived interest to these sources [21–36]. The CS source is based on a collision of a laser pulse with a relativistic electron beam [Fig. 1(a)]. While not competing with brightness of large facilities, CS sources have several advantages, providing x-ray photons at a tunable energy in a broad spectral range, and being relatively compact and affordable.

A compact brilliant x-ray light source with narrow bandwidth (BW) is an attractive tool, e.g., for x-ray imaging in biology [37], x-ray nanoscale diagnostics in material science [38–40], x-ray spectroscopy of highly charged ions [41, 42]. Recently a new field of x-ray quantum optics has been advanced aimed at the coherent control of atomic nuclei using shaped resonant x-rays [43–49], which requires especially narrow BW x-ray beams. Different schemes for narrowing the x-ray BW have been proposed involving temporal laser pulse chirping [28–33], or temporally varying polarization [34] to compensate the nonlinear spectrum broadening. Alternatively, the x-ray photon yield at low BW can be enhanced using a traveling-wave setup which allows an overlap of electron and laser beams longer than the Rayleigh length [35, 36]. However, all these approaches require the precise control of the pulse shape, phase or polarization, which is difficult in the high intensity domain.

In this Letter an alternative approach for narrow BW bright x-rays is put forward. Rather than modifying the laser pulse, an additional laser beam co-propagating with the electrons is introduced. Namely, the setup consists of a relativistic electron beam interacting with two counterpropagating waves (CPW) [Fig. 1(b)]. The electron motion features two typical frequencies, separated by orders of magnitude because of the Doppler effect,  $\omega_1 = \omega_0(1 + v_z) \approx 2\omega_0$  and  $\omega_2 = \omega_0(1 - v_z) \approx \omega_0/2\gamma_*^2$

where  $\omega_0$  is the laser frequency and  $v_z$  the relativistic average velocity on axis and  $\gamma_*$  the effective Lorentz factor [50] (units  $\hbar = c = 1$  are used throughout). Due to the nonlinearity of the relativistic dynamics the electron absorbs several photons in both frequencies in the considered regime when emitting an x-ray photon. As a result in the emission spectrum the Doppler-shifted high frequency  $\omega_1$  peak is accompanied with satellites of  $\omega_0$  separation. While the gross features of the spectrum (the spectral envelope) are determined by the counterpropagating laser beam, the subtle features are governed by the second co-propagating laser beam. Accordingly, the BW of satellites scales with the smaller frequency  $\omega_2$ , allowing for bright ultranarrow BW x-rays.

The radiation has been calculated employing the Baier-Katkov semiclassical operator method [51], applicable when the electron dynamics is quasiclassical in strong background fields. The radiation spectrum reads [52, 53]:

$$dI = \frac{\alpha}{(2\pi)^2\tau} \left[ -\frac{\varepsilon'^2 + \varepsilon^2}{2\varepsilon'^2} |\mathcal{T}_\mu|^2 + \frac{m^2\omega^2}{2\varepsilon'^2\varepsilon^2} |I|^2 \right] d^3\mathbf{k}', \quad (1)$$

where  $I \equiv \int_{-\infty}^{\infty} e^{i\psi} dt$ ,  $\mathcal{T}_\mu \equiv \int_{-\infty}^{\infty} v_\mu(t) e^{i\psi} dt$ ,  $\psi \equiv \frac{\varepsilon}{\varepsilon'} \mathbf{k}' \cdot \mathbf{x}(t)$  is the emission phase, and  $x_\mu(t)$ ,  $v_\mu(t)$ ,  $k'_\mu = (\omega', \mathbf{k}')$  are the four-vectors of the electron coordinate, the velocity and the emitted photon momentum, respectively.  $\tau$  is the pulse duration,  $\varepsilon$  the electron energy with  $\varepsilon' = \varepsilon - \omega'$ . In our setup ultrarelativistic electrons counterpropagate to the circularly polarized laser field with a vector-potential  $A_1(x, t) = m\xi_1[\cos(k_1 \cdot x)e_x + \sin(k_1 \cdot x)e_y]$ , where  $\xi_1 = eE_0/(m\omega_0)$ ,  $E_0$  and  $\omega_0$  are the laser field amplitude and frequency, respectively.  $k_1 = (\omega_0, 0, 0, -\omega_0)$  is the laser four-wave vector with  $\omega_0 = 1.55$  eV, and  $e_x = (0, 1, 0, 0)$ ,  $e_y = (0, 0, 1, 0)$ .  $-e$  and  $m$  are the electron charge and mass, respectively. The second laser field co-propagating with the electrons is also circularly polarized:  $A_2(x, t) = m\xi_2[\cos(k_2 \cdot x)e_x + \sin(k_2 \cdot x)e_y]$ , with  $k_2 = (\omega_0, 0, 0, \omega_0)$ . The two lasers have the same frequency  $\omega_0$  in the Lab-frame. We keep  $\xi_1 < 1$ , namely  $\xi_1 = 0.1$ , while choosing either  $\xi_2 < \xi_1$  (Case I,  $\xi_2 = 0.02$ ) or  $\xi_2 > \xi_1$  (Case II,  $\xi_2 = 2$ ). The quantum strong-field parameter  $\chi = e\sqrt{-(F^{\mu\nu}P_\nu)^2}/m^3$ , with the field tensor  $F^{\mu\nu}$ , and four-momentum  $P_\nu$ , is small  $\chi \sim 10^{-5}$  for the chosen param-

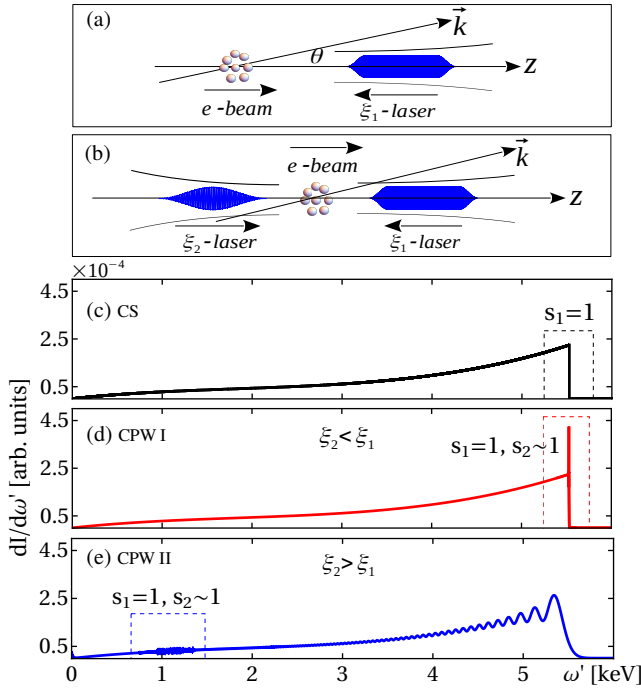


Figure 1. The setup of a relativistic electron beam colliding with a single laser pulse for CS (a), and with CPW (b). The emission spectra for CS (c), for Case I (d), and Case II (e). The electron energy is  $\varepsilon = 30m$  in all cases.  $s_i$  denotes the absorbed photon numbers from the laser  $\xi_i$  ( $i = 1, 2$ ), respectively.

ters, and multiple photon emissions are negligible.

The radiation spectra are presented in Fig. 1. The general features of all the spectra are similar. In the CS case,  $\xi_2 = 0$  [Fig. 1(c)], the spectrum has a sharp edge corresponding to absorption of a single photon (as  $\xi_1 < 1$ ) from the laser field. The same edge is also dominant in spectra for cases I and II in CPW, because  $\chi$ , determining the general spectral shape, is dominated by the  $\xi_1$ -laser. However, the details of the spectra in CPW reveal features stemming from the  $\xi_2$ -laser which are absent in CS. For Case I [Fig. 1(d)] a single but ultra-narrow harmonic rises with a similar location but larger strength near the spectrum edge. For Case II [Fig. 1(e)] the entire spectrum becomes oscillatory and in most of the energy domain these oscillations are quite wide. However, the radiation emitted on axis, corresponding to  $s_2 \sim 1$ , exhibits a comb of sharp peaks, which is the main interest here and discussed below.

The angle-resolved spectra are presented in Fig. 2 for CS and CPW Case I, and Fig. 3 for CPW Case II. While in the CS case a single harmonic appears in the given limited spectral range [Fig. 2(a)], in CPW many satellites accompany the given harmonic due to absorption of additional photons from the  $\xi_2$  laser [Figs. 2(d) and 3(a)]. Generally the radiation is distributed in a rather large angle and frequency region. Since  $\xi_1 < 1$ , the photon number for both CS and Case I in CPW decreases monotonically in the  $1/\gamma$ -cone, while the BW increases with  $\theta$  until it reaches a constant value [50]. This makes the brilliance for

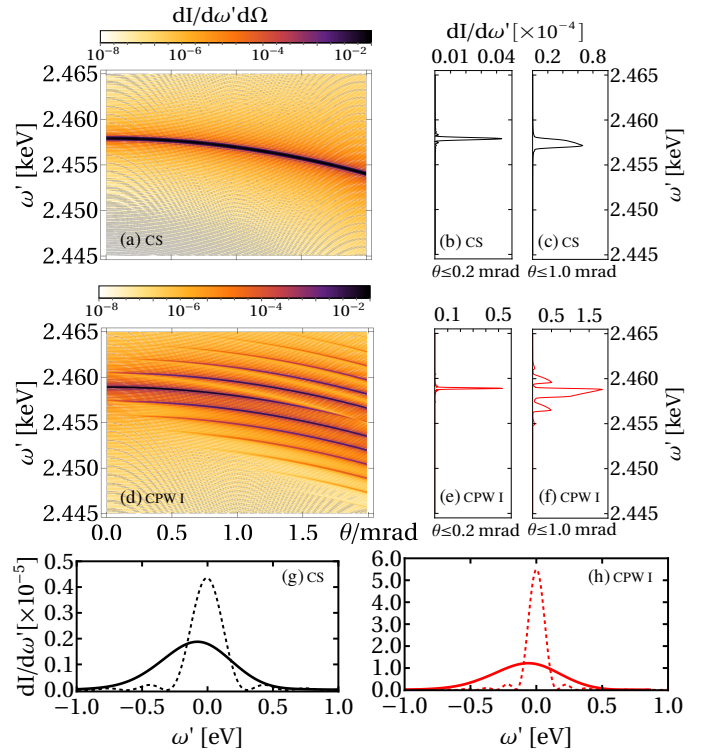


Figure 2. The angle-resolved spectra: (a) CS; (d) CPW Case I. The angle integrated spectra: within  $\theta \leq 0.2$  mrad for (b) CS; (e) CPW Case I and within  $\theta \leq 1$  mrad for (c) CS; (f) CPW Case I. The spectra from a realistic electron beam (solid) and a monochromatic electron beam (dashed): (g) for CS; (h) for CPW Case I. The x-axis in panels (g,h) has been shifted by the peak energy in (b) and (e), respectively. The electron beam has a Gaussian distribution in both angle ( $\Delta\theta = 1$  mrad) and energy (0.01% relative FWHM) domain with central energy  $\varepsilon = 20m$ . The pulse length for  $\xi_1$  is 16000 cycles while the pulse length for  $\xi_2$  is the same as the electron beam length, which is about 750 cycles.

both cases being the largest in the forward direction. Moreover, by integrating over the same angle range around  $\theta = 0$ , we can see that the radiation in Case I is narrower in BW and more intense compared with CS [Fig. 2(b,e)], which finally results in higher brilliance. After taking into account that the energy spreading and emittance of a realistic electron beam broaden the emission BW [Fig. 2(g,h)], the advantage of Case I in brilliance compared to CS still remains at about one order of magnitude.

Furthermore, a comb-like structure is produced in Case II [Fig. 3(b,c)]. While state-of-the-art techniques for a frequency comb can achieve the XUV domain [54–57], the covet is the hard x-ray regime. An attempt in this direction recently shown in [34] via CS with a polarization gating, demonstrated a relative BW of  $10^{-2}$  and the spacing between peaks of the order of  $\sim 100$  keV. In our CPW setup, however, the comb spacing is at an optical frequency, with more than one order of magnitude smaller relative BW [Fig. 3(d)].

These results raise several questions: i) What determines the peak locations and the spacing between sequential peaks? ii)

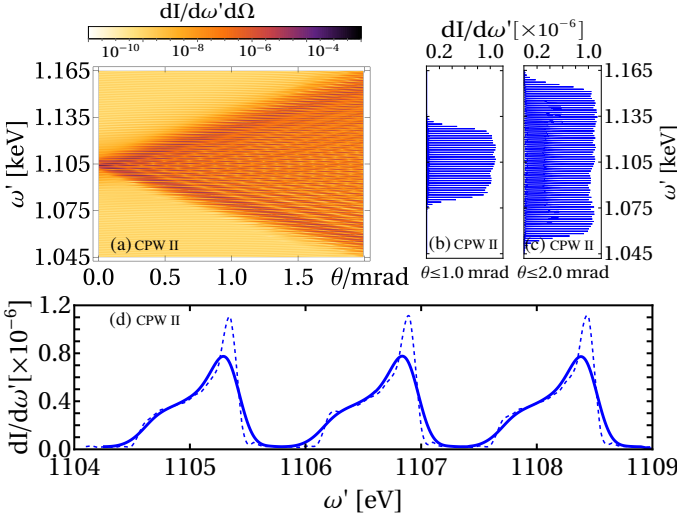


Figure 3. (a) The angle-resolved spectra for CPW Case II. The angle integrated spectra for CPW Case II: (b) within  $\theta \leq 1$  mrad; (c) within  $\theta \leq 2$  mrad; (d) The spectrum from a realistic electron beam for CPW Case II (solid) and a monochromatic electron beam (dashed). The electron beam has the same distributions as in Fig. 2, but with central energy  $\varepsilon = 30m$ . The pulse length for  $\xi_1$  is 8000 cycles while the pulse length for  $\xi_2$  is the same as the electron beam length, which is about 750 cycles.

What determines the width of a single peak? iii) What is the role played by the angle window? and iv) How can we control the number of harmonics contained in the spectrum? To address them, we turn to analytical estimations. The emission phase is a key variable  $\psi = \psi_{np}t - z_1 \sin \omega_1 t - z_2 \sin \omega_2 t - z_3 \sin \Delta\omega_{12}t$ , with  $\psi_{np} = \varepsilon u(1 - v_z \cos \theta)$ ,  $z_1 = (m\xi_1 u/\omega_1) \sin \theta$ ,  $z_2 = (m\xi_2 u/\omega_2) \sin \theta$ ,  $z_3 = 2\omega_0 m^2 \xi_1 \xi_2 u/(\varepsilon \Delta\omega_{12}^2)$ ,  $\Delta\omega_{12} = \omega_1 - \omega_2$ , and  $u = \omega'/(\varepsilon - \omega')$ . The integral in Eq. (1) over this phase yields multiplications of Bessel functions with arguments  $z_1, z_2, z_3$  [52, 53]. From the phase follows the energy-momentum conservation, determining the emitted photon energy [50]:

$$\omega' = \frac{\omega_{s_1, s_2}^m}{1 + 2\gamma_*^2(1 - \cos \theta)}, \quad (2)$$

where  $\omega_{s_1, s_2}^m = 2\gamma_*^2(s_1\omega_1 + s_2\omega_2)$  with  $s_1, s_2$  being the numbers of photons absorbed from the first and second pulse, respectively, and  $\gamma_* = \varepsilon/m_*$ , with the effective mass  $m_* \equiv m\sqrt{1 + \xi_1^2 + \xi_2^2}$ . The spacing between sequential  $s_2$  harmonics according to Eq. (2) is  $\Delta\omega' = 2\gamma_*^2\omega_2 \approx \omega_0$ , because  $\omega_1/\omega_2 \approx 4\gamma_*^2$  and  $\omega_1 = 2\omega_0$ . The rather broad emission frequency region in Figs. 2 and 3 follows from Eq. (2). Each line in Figs. 2(d) and 3(a) represents the location of a single harmonic with respect to  $\omega_2$ . The spacing between adjacent lines is  $\omega_0$ .

To obtain a narrow BW radiation, one needs to apply the emission angle window ( $\Delta\theta_w$ ). The width of the harmonic due

to this finite angle window based on Eq. (2) is

$$\delta\omega'_w = \omega_{s_1, s_2}^m (\gamma_* \Delta\theta_w)^2. \quad (3)$$

In both cases, CS and CPW, the most beneficial for a small BW is the region near forward direction ( $\theta = 0$ ), when  $\partial\omega'/\partial\theta = 0$ . Then, at applying a rather small angle window  $\Delta\theta_w$ , the BW is not  $\Delta\theta_w$ -dependent, but determined by the dynamical linewidth. The latter is smaller for CPW in comparison to CS.

The dynamical width of the harmonics is affected by two factors. The first stems from the characteristics of the electron dynamics. From the Bessel function features, the CPW harmonic width is estimated via  $z_2 \approx 1$  [50]. For the main peak

$$\delta\omega'_c = \frac{\omega_2}{8} \left( \frac{m_*}{m\xi_2} \right)^2. \quad (4)$$

The latter BW scaling is surprising. In contrast to CS, the harmonics become narrower for increasing electron energy, confirmed with numerical calculations [50]. For the considered parameters  $\delta\omega'_c \ll \omega_0$ , which results in an enhancement of satellite peaks over the spectral CS envelope. In fact, adding the second laser  $\xi_2$  to the CS setup, new satellite peaks arise with a  $\omega_0$  separation, and the smooth energy distribution within a large BW for CS,  $\delta\omega'_{CS} \sim \omega_0\gamma^2/\xi_1^2$  [50], roams into sharp spikes.

The second contribution to the harmonic width arises from the finite duration of the laser pulses. Note that the duration of the first pulse should be much longer,  $N_1 = nN_2$ , where  $n = \omega_1/\omega_2$ , and  $N_{1,2}$  are the numbers of cycles experienced by a single electron during the interaction. Therefore, the photon uncertainty width is mostly determined by the second pulse

$$\delta\omega'_f = 2\gamma_*^2\omega_2/N_2 = \omega_0/N_2. \quad (5)$$

Controlling the angle range  $\Delta\theta_w$ , one can tune  $\delta\omega'_w$  mentioned above such as not to exceed the dynamical width:  $\delta\omega'_{in} = \max(\delta\omega'_c, \delta\omega'_f)$  [50]. Please note that the pulse length for  $\xi_2$  and the electron beam in a realistic experimental setup should be similar such that all the electrons in the beam will contribute to the emitted x-ray pulse during the interaction [50].

In Case II [Fig. 3], the photon energy  $\omega'$  is less sensitive to the emission angle than in Case I because of a smaller velocity  $v_z$  at the same energy (at different effective masses) and the number of harmonics is significantly larger than in Case I because  $m_*/m\xi_2 \approx \xi_1/\xi_2 \ll 1$ . We can assess the effective number of harmonics  $\Delta s_2$  for a given angle window  $\Delta\theta_w$  by requiring  $z_2/\Delta s_2 = \delta$ , with a choice  $\delta \approx 0.8$ , according to the Bessel function properties [50]:

$$\Delta s_2 \approx \frac{1}{\delta} \left( \frac{\Delta\theta_w}{\theta_c} \right), \quad \theta_c = \frac{m_*}{8m\xi_2\gamma_*^3} \quad (6)$$

where  $\theta_c$  corresponds to the angle when  $\delta\omega'_w(\theta_c)$  is equal to the characteristic width of the harmonics. The integrated spectra over a different angle range in Fig. 3(b,c) for Case II reveals a trade-off. On the one hand, the range of the comb can be extended by increasing the angle window. On the other hand,

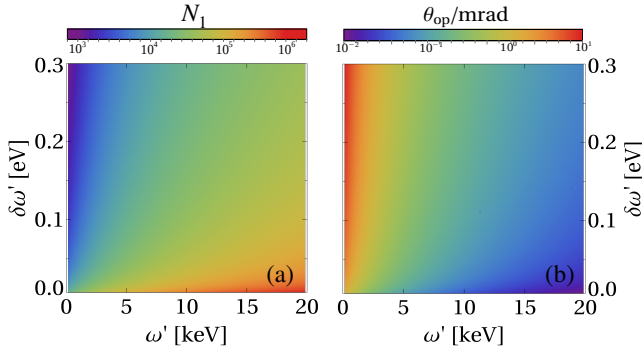


Figure 4. (a) the required pulse length  $N_1$  of the  $\xi_1$  laser for different emitted photon energies  $\omega'$  with different harmonic peak widths  $\delta\omega'$  in the spectrum. (b) the optimized angle range  $\theta_{op}$  for different emitted photon energies  $\omega'$  with different harmonic peak widths  $\delta\omega'$  when we choose the pulse length in panel (a).

it also induces a larger background in the gap between two sequential harmonics[50]. One should balance between the width of a single harmonic and the range of the total comb to have an optimized x-ray comb.

The emittance and energy spreading of the electron beam will cause broadening of the radiation BW and suppress the brilliance. Is it possible with a realistic electron beam in the CPW setup to obtain brilliance better than in CS and generate the comb structure? From Eq. (2) we may estimate the contribution of energy  $\Delta\gamma/\gamma$  and angular  $\Delta\theta$  spread in the BW broadening as  $\delta\omega'/\omega' \sim \max\{\Delta\gamma/\gamma, (\gamma\Delta\theta)^2\}$ . Using electron beam parameters envisaged in [58]:  $\Delta\gamma/\gamma \sim 10^{-4}$  and  $\Delta\theta \approx p_\perp/p_z \sim 10^{-3}$ , we can expect the BW broadening up to  $\delta\omega'/\omega' \sim 10^{-4}$ . We have tested our conclusion by numerical calculations of the spectra for an electron beam having a Gaussian distribution in both energy and angle domain with relative FWHM equal to  $10^{-4}$  and  $10^{-3}$ , respectively [Figs. 2(g,h),3(d)]. Let us discuss the brilliance issue. The brilliance for both CPW and CS cases are the largest in the forward direction [50]. In the case of angle window  $\Delta\theta_w = 0.2$  mrad in the forward direction [Fig. 2(b,e)], the relative BW in CS for a single electron is  $\Delta\omega'/\omega' \approx 10^{-4}$ , while in CPW Case I it is 2 times smaller due to smallness of the dynamical BW. However, the number of photons in the line in the CPW case is about 7 times larger than in CS, which is due to more prominent forward emission in CPW. In the case of the electron beam with above parameters, the BW for CS is 1.4 times larger than for CPW, leaving however, the number of photons in the emission line equal to the case without spreading. Thus, we can have an order of magnitude larger brilliance in the CPW Case I with respect to CS with the same laser and electron parameters. For instance using electron beam with 10pC charge and emittance of 0.1 mm-mrad (with angle spreading  $\Delta\theta = 1$  mrad and transverse radius of 0.1 mm) and 0.01% energy spreading at electron energy  $\varepsilon = 10$  MeV [58] the peak brilliance in forward direction for the CPW Case I  $\mathcal{B} \sim 5.2 \times 10^{18}$  ph/(s-mrad<sup>2</sup>·mm<sup>2</sup>·0.1%BW), while in CS it is  $\mathcal{B} \sim 6.5 \times 10^{17}$  ph/(s-mrad<sup>2</sup>·mm<sup>2</sup>·0.1%BW).

The comb-like structure is also preserved when using the electron beam with spreading parameters as above. Thus, Fig. 3(d) shows that in the case of an angular window  $\Delta\theta_w = 2$  mrad the electron beam spreading induces a 2 times increase of BW. However, the comb structure, with numbers of peaks in the comb  $\Delta s_2 = 70$  is still preserved, characterized by the comb visibility, ratio of the BW to the peak separation, being equal to 0.37. The decrease of the angle window will improve the comb visibility, but will decrease the comb length.

Summarizing our approach, firstly, configuration I or II is chosen depending on the preference of the spectral shape: a single peak or a frequency comb. Then, the desired energy location and width are specified. The energy  $\omega'$  determines the effective relativistic factor  $\gamma_*$  via Eq. (2). Then, from the chosen width  $\delta\omega'$  and relation (3), the angle window  $\theta_w$  follows. For Case II, where  $\delta\omega'_f$  dominates  $\delta\omega'_{in}$ , we also require  $\delta\omega'_f = \delta\omega'$ , from which the duration of the second pulse is evaluated. For a given laser pulse energy and the pulse duration the field amplitude is derived, which determines the effective mass, and from  $\gamma_*$  one finds the electron energy [Fig. 4]. For a given BW, the number of cycles is determined according to Eq. (5). However, increasing  $\omega'$  requires a longer duration of the first pulse, due to increase of  $n = \omega_1/\omega_2 \approx 4\gamma_*^2$ . The optimal angle window  $\theta_w$  according to Eq. (2) is narrower at higher  $\omega'$ .

In conclusion, the discussed CPW setup allows to generate an extremely narrow BW and collimated x-ray beam in the range of several hundreds of eV to tens of keV, with brilliance by an order of magnitude exceeding that for CS corresponding to the same laser and electron beam parameters. By tuning the intensity of the two laser pulses, one can produce either a single peak or a comb-like x-ray source. This radiation source is attractive for several applications. First, its narrow-band features allow for resonant excitation spectroscopy of highly charged ions [41, 42, 59–61], without the use of a monochromator as opposed to synchrotron sources. Furthermore, by utilizing the comb, one can probe a much larger energy range in a single shot. Second, the flux and BW of this source render it suitable to operate it as an XFEL seeder, thus replacing the complex and cumbersome self-seeding unit [62–64], which is the only available seeding technique above energies of 100 eV. Third, owing to the low angle spread it is favourable as a source for small angle scattering diagnostics [39]. Fourth, the comb-like structure can be employed for extension of plasma diagnostics from the optical and UV range [65–67] to the hard x-ray domain, e.g., for a temporally resolved measurement of the density profile of overdense plasmas. The proposed x-ray comb-structure will enable probing much higher density plasma in a large density range in a single shot, with high accuracy due to the ultra-narrow BW of the single peak in the comb. Finally, replacing the laser fields with strong THz ones, the presented idea can be extended to a hard x-ray frequency comb for ultrahigh precision metrology.

Q.Z.L wishes to thank Zoltán Harman for helpful discussions regarding the applications of the x-ray frequency comb structure. We all thank Jörg Evers for useful comments on this Letter.

\* qingzheng.lyu@mpi-hd.mpg.de

† erez.raicher@mail.huji.ac.il

- [1] B. M. Murphy O. H. Seeck, ed., *X-ray diffraction: Modern experimental technique* (Taylor and Francis Group, 2014) p. 420.
- [2] Carlos Sanchez-Cano, Ramon A. Alvarez-Puebla, John M. Abendroth, Tobias Beck, Robert Blick, Yuan Cao, Frank Caruso, Indranath Chakraborty, Henry N. Chapman, Chunying Chen, Bruce E. Cohen, Andre L. C. Conceição, David P. Cormode, Daxiang Cui, Kenneth A. Dawson, Gerald Falkenberg, Chunhai Fan, Neus Feliu, Mingyuan Gao, Elisabetta Gargioni, Claus-C. Glüer, Florian Grüner, Moustapha Hassan, Yong Hu, Yalan Huang, Samuel Huber, Nils Huse, Yanan Kang, Ali Khademhosseini, Thomas F. Keller, Christian Körnig, Nicholas A. Kotov, Dorota Koziej, Xing-Jie Liang, Beibei Liu, Sijin Liu, Yang Liu, Ziyao Liu, Luis M. Liz-Marzán, Xiaowei Ma, Andres Machicote, Wolfgang Maisson, Adrian P. Mancuso, Saad Megahed, Bert Nickel, Ferdinand Otto, Cristina Palencia, Sakura Pascarelli, Arwen Pearson, Oula Peñate-Medina, Bing Qi, Joachim Rädler, Joseph J. Richardson, Axel Rosenhahn, Kai Rothkamm, Michael Rübhausen, Milan K. Sanyal, Raymond E. Schaak, Heinz-Peter Schlemmer, Marius Schmidt, Oliver Schmutzler, Theo Schotten, Florian Schulz, A. K. Sood, Kathryn M. Spiers, Theresa Staufer, Dominik M. Stemer, Andreas Stierle, Xing Sun, Gohar Tsakanova, Paul S. Weiss, Horst Weller, Fabian Westermeier, Ming Xu, Huijie Yan, Yuan Zeng, Ying Zhao, Yuliang Zhao, Dingcheng Zhu, Ying Zhu, and Wolfgang J. Parak, “X-ray-Based Techniques to Study the Nano–Bio Interface,” *ACS Nano* **15**, 3754–3807 (2021).
- [3] I. M. Ternov, “Synchrotron radiation,” *Sov. Phys.-Uspekhi* **38**, 409–434 (1995).
- [4] K Wille, “Synchrotron radiation sources,” *Reports on Progress in Physics* **54**, 1005–1067 (1991).
- [5] T Nakazato, M Oyamada, N Niimura, S Urasawa, O Konno, A Kagaya, R Kato, T Kamiyama, Y Torizuka, T Nanba, *et al.*, “Observation of coherent synchrotron radiation,” *Physical review letters* **63**, 1245 (1989).
- [6] H.-P. Schlenvoigt, K. Haupt, A. Debus, F. Budde, O. Jäckel, S. Pfotenhauer, H. Schwoerer, E. Rohwer, J. G. Gallacher, E. Brunetti, R. P. Shanks, S. M. Wiggins, and D. A. Jaroszynski, “A compact synchrotron radiation source driven by a laser-plasma wakefield accelerator,” *Nature Phys.* **4**, 130 (2008).
- [7] Henry N. Chapman, “X-ray imaging beyond the limits,” *Nature Materials* **8**, 299–301 (2009).
- [8] C Pellegrini, A Marinelli, and S Reiche, “The physics of x-ray free-electron lasers,” *Reviews of Modern Physics* **88**, 015006 (2016).
- [9] Christoph Bostedt, Sébastien Boutet, David M Fritz, Zhirong Huang, Hae Ja Lee, Henrik T Lemke, Aymeric Robert, William F Schlotter, Joshua J Turner, and Garth J Williams, “Linac coherent light source: The first five years,” *Reviews of Modern Physics* **88**, 015007 (2016).
- [10] The European X-Ray Laser Project XFEL, (2011).
- [11] The Linac Coherent Laser Source (LCLS), (2011).
- [12] Zhentang Zhao, Dong Wang, Qiang Gu, Lixin Yin, Guoping Fang, Ming Gu, Yongbin Leng, Qiaogen Zhou, Bo Liu, Chuanxiang Tang, *et al.*, “Sxfel: A soft x-ray free electron laser in china,” *Synchrotron Radiation News* **30**, 29–33 (2017).
- [13] A. Ting, R. Fischer, A. Fisher, K. Evans, R. Burris, J. Krall, E. Esarey, and P. Sprangle, “Observation of 20 ev x-ray generation in a proof-of-principle laser synchrotron source experiment,” *J. Appl. Phys.* **78** (1995).
- [14] R. W. Schoenlein, W. P. Leemans, A. H. Chin, P. Volfbeyn, T. E. Glover, P. Balling, M. Zolotarev, K.-J. Kim, S. Chattopadhyay, and C. V. Shank, “Femtosecond x-ray pulses at 0.4 Å generated by 90° thomson scattering: A tool for probing the structural dynamics of materials,” *Science* **274**, 236–238 (1996).
- [15] I. Sakai, T. Aoki, K. Dobashi, M. Fukuda, A. Higurashi, T. Hirose, T. Iimura, Y. Kurihara, T. Okugi, T. Omori, J. Urakawa, M. Washio, and K. Yokoya, “Production of high brightness gamma-rays through backscattering of laser photons on high-energy electrons,” *Phys. Rev. ST AB* **6**, 091001 (2003).
- [16] David J. Gibson, Scott G. Anderson, Christopher P. J. Barty, Shawn M. Betts, Rex Booth, Winthrop J. Brown, John K. Crane, Robert R. Cross, David N. Fittinghoff, Fred V. Hartemann, Jaroslav Kuba, Gregory P. Le Sage, Dennis R. Slaughter, Aaron M. Tremaine, Alan J. Wootton, Edward P. Hartouni, Paul T. Springer, and James B. Rosenzweig, “Pleiades: A picosecond compton scattering x-ray source for advanced backlighting and time-resolved material studies,” *Phys. Plasmas* **11**, 2857–2864 (2004).
- [17] Antoine Rousse, Kim Ta Phuoc, Rahul Shah, Alexander Pukhov, Eric Lefebvre, Victor Malka, Sergey Kiselev, Frédéric Burgy, Jean-Philippe Rousseau, Donald Umstadter, and Danièle Hulin, “Production of a kev x-ray beam from synchrotron radiation in relativistic laser-plasma interaction,” *Phys. Rev. Lett.* **93**, 135005 (2004).
- [18] S. Corde, K. Ta Phuoc, G. Lambert, R. Fitour, V. Malka, A. Rousse, A. Beck, and E. Lefebvre, “Femtosecond x rays from laser-plasma accelerators,” *Rev. Mod. Phys.* **85**, 1–48 (2013).
- [19] Alberto Benedetti, Matteo Tamburini, and Christoph H Keitel, “Giant collimated gamma-ray flashes,” *Nature Photonics* **12**, 319–323 (2018).
- [20] Archana Sampath, Xavier Davoine, Sébastien Corde, Laurent Gremillet, Max Gilljohann, Maitreyi Sangal, Christoph H Keitel, Robert Ariniello, John Cary, Henrik Ekerfelt, *et al.*, “Extremely dense gamma-ray pulses in electron beam-multifoil collisions,” *Physical Review Letters* **126**, 064801 (2021).
- [21] Frederic V Hartemann, Félicie Albert, Craig W Siders, and C.P.J. Barty, “Low-intensity nonlinear spectral effects in compton scattering,” *Physical review letters* **105**, 130801 (2010).
- [22] Geoffrey A Krafft and Gerd Priebe, “Compton sources of electromagnetic radiation,” *Reviews Of Accelerator Science And Technology: Volume 3: Accelerators as Photon Sources*, 147–163 (2010).
- [23] Chao Chang, Chuanxiang Tang, and Juhao Wu, “High-gain thompson-scattering x-ray free-electron laser by time-synchronic laterally tilted optical wave,” *Phys. Rev. Lett.* **110**, 064802 (2013).
- [24] S. Chen, N. D. Powers, I. Ghebregziabher, C. M. Maharjan, C. Liu, G. Golovin, S. Banerjee, J. Zhang, N. Cunningham, A. Moorti, S. Clarke, S. Pozzi, and D. P. Umstadter, “MeV-energy x rays from inverse compton scattering with laser-wakefield accelerated electrons,” *Phys. Rev. Lett.* **110**, 155003 (2013).
- [25] Fred V. Hartemann and Sheldon S. Q. Wu, “Nonlinear brightness optimization in compton scattering,” *Phys. Rev. Lett.* **111**, 044801 (2013).
- [26] G. Sarri, D. J. Corvan, W. Schumaker, J. M. Cole, A. Di Piazza, H. Ahmed, C. Harvey, C. H. Keitel, K. Krushelnick, S. P. D. Mangles, Z. Najmudin, D. Symes, A. G. R. Thomas, M. Yeung, Z. Zhao, and M. Zepf, “Ultrahigh brilliance multi-mev gamma-ray beams from nonlinear relativistic thomson scattering,” *Phys. Rev. Lett.* **113**, 224801 (2014).
- [27] K. Khrennikov, J. Wenz, A. Buck, J. Xu, M. Heigoldt, L. Veisz, and S. Karsch, “Tunable all-optical quasimonochromatic thomson x-ray source in the nonlinear regime,” *Phys. Rev. Lett.* **114**, 195003 (2015).

- [28] Isaac Ghebregziabher, B. A. Shadwick, and Donald Umstadter, “Spectral bandwidth reduction of thomson scattered light by pulse chirping,” *Phys. Rev. ST Accel. Beams* **16**, 030705 (2013).
- [29] Balša Terzić, Kirsten Deitrick, Alicia S Hofer, and Geoffrey A Krafft, “Narrow-band emission in thomson sources operating in the high-field regime,” *Physical review letters* **112**, 074801 (2014).
- [30] D Seipt, SG Rykovanov, A Surzhykov, and S Fritzsche, “Narrowband inverse compton scattering x-ray sources at high laser intensities,” *Physical Review A* **91**, 033402 (2015).
- [31] Vasily Yu Kharin, Daniel Seipt, and Sergey G Rykovanov, “Higher-dimensional caustics in nonlinear compton scattering,” *Physical review letters* **120**, 044802 (2018).
- [32] C Maroli, V Petrillo, I Drebot, L Serafini, B Terzić, and GA Krafft, “Compensation of non-linear bandwidth broadening by laser chirping in thomson sources,” *Journal of Applied Physics* **124**, 063105 (2018).
- [33] Daniel Seipt, Vasily Yu Kharin, and Sergey G Rykovanov, “Optimizing laser pulses for narrow-band inverse compton sources in the high-intensity regime,” *Physical review letters* **122**, 204802 (2019).
- [34] MA Valialshchikov, V Yu Kharin, and SG Rykovanov, “Narrow bandwidth gamma comb from nonlinear compton scattering using the polarization gating technique,” *Physical Review Letters* **126**, 194801 (2021).
- [35] A.D. Debus, M. A Bussmann, M. A Siebold, A. A Jochmann, U. A Schramm, T.E. A Cowan, and R. A Sauerbrey, “Traveling-wave thomson scattering and optical undulators for high-yield euv and x-ray sources,” *Appl. Phys. B* **100**, 61 (2010).
- [36] A. Jochmann, A. Irman, M. Bussmann, J. P. Couperus, T. E. Cowan, A. D. Debus, M. Kuntzsch, K. W. D. Ledingham, U. Lehnert, R. Sauerbrey, H. P. Schlenvoigt, D. Seipt, Th. Stöhler, D. B. Thorn, S. Trotsenko, A. Wagner, and U. Schramm, “High resolution energy-angle correlation measurement of hard x rays from laser-thomson backscattering,” *Phys. Rev. Lett.* **111**, 114803 (2013).
- [37] Frank E Carroll, Marcus H Mendenhall, Robert H Traeger, Charles Brau, and James W Waters, “Pulsed tunable monochromatic x-ray beams from a compact source: new opportunities,” *American journal of roentgenology* **181**, 1197–1202 (2003).
- [38] DCF Wieland, MA Schroer, A Yu Gruzinov, CE Blanchet, CM Jeffries, and DI Svergun, “Asaxs measurements on ferritin and apoferritin at the biosaxs beamline p12 (petra iii, desy),” *Journal of Applied Crystallography* **54** (2021).
- [39] Tao Li, Andrew J Senesi, and Byeongdu Lee, “Small angle x-ray scattering for nanoparticle research,” *Chemical reviews* **116**, 11128–11180 (2016).
- [40] Greg L Hura, Angeli L Menon, Michal Hammel, Robert P Rambo, Farris L Poole Ii, Susan E Tsutakawa, Francis E Jenney Jr, Scott Classen, Kenneth A Frankel, Robert C Hopkins, *et al.*, “Robust, high-throughput solution structural analyses by small angle x-ray scattering (saxs),” *Nature methods* **6**, 606–612 (2009).
- [41] Sven Bernitt, GV Brown, Jan K Rudolph, R Steinbrügge, A Graf, M Leutenegger, SW Epp, Sita Eberle, K Kubiček, Volkhard Mäkel, *et al.*, “An unexpectedly low oscillator strength as the origin of the fe xvii emission problem,” *Nature* **492**, 225–228 (2012).
- [42] Steffen Kühn, Chintan Shah, José R Crespo López-Urrutia, Keisuke Fujii, René Steinbrügge, Jakob Stierhof, Moto Togawa, Zoltán Harman, Natalia S Oreshkina, Charles Cheung, *et al.*, “High resolution photoexcitation measurements exacerbate the long-standing fe xvii oscillator strength problem,” *Physical review letters* **124**, 225001 (2020).
- [43] Thomas J Bürvenich, Jörg Evers, and Christoph H Keitel, “Nuclear quantum optics with x-ray laser pulses,” *Physical review letters* **96**, 142501 (2006).
- [44] Ralf Röhlberger, Hans-Christian Wille, Kai Schlage, and Balam Sahoo, “Electromagnetically induced transparency with resonant nuclei in a cavity,” *Nature* **482**, 199–203 (2012).
- [45] K P Heeg, A Kaldun, C Strohm, P Reiser, C Ott, R Subramanian, D Lentrodt, J Haber, H-C Wille, S Goerttler, R Ruffer, C H Keitel, R Röhlberger, T Pfeifer, and J Evers, “Spectral narrowing of x-ray pulses for precision spectroscopy with nuclear resonances,” *Science (New York, N.Y.)* **357**, 375–378 (2017).
- [46] Kilian P. Heeg, Andreas Kaldun, Cornelius Strohm, Christian Ott, Rajagopalan Subramanian, Dominik Lentrodt, Johann Haber, Hans-Christian Wille, Stephan Goerttler, Rudolf Ruffer, Christoph H. Keitel, Ralf Röhlberger, Thomas Pfeifer, and Jörg Evers, “Coherent X-ray-optical control of nuclear excitons,” *Nature* **590**, 401–404 (2021).
- [47] Farit Vagizov, Vladimir Antonov, YV Radeonychev, RN Shakhmuratov, and Olga Kocharovskaya, “Coherent control of the waveforms of recoilless  $\gamma$ -ray photons,” *Nature* **508**, 80–83 (2014).
- [48] Aleksandr I Chumakov, Alfred QR Baron, Ilya Sergueev, Cornelius Strohm, Olaf Leupold, Yuri Shvyd’ko, Gennadi V Smirnov, Rudolf Ruffer, Yuichi Inubushi, Makina Yabashi, *et al.*, “Superradiance of an ensemble of nuclei excited by a free electron laser,” *Nature Physics* **14**, 261–264 (2018).
- [49] Elena Kuznetsova and Olga Kocharovskaya, “Quantum optics with x-rays,” *Nature Photonics* **11**, 685–686 (2017).
- [50] See the Supplemental Materials for the details.
- [51] V. N. Baier, V. M. Katkov, and V. M. Strakhovenko, *Electromagnetic Processes at High Energies in Oriented Single Crystals* (World Scientific, Singapore, 1994).
- [52] Q. Z. Lv, E. Raicher, C. H. Keitel, and K. Z. Hatsagortsyan, “Anomalous violation of the local constant field approximation in colliding laser beams,” *Physical Review Research* **3**, 013214 (2021).
- [53] Q Z Lv, E Raicher, C H Keitel, and K Z Hatsagortsyan, “Ultra-relativistic electrons in counterpropagating laser beams,” *New Journal of Physics* **23**, 065005 (2021).
- [54] Christoph Gohle, Thomas Udem, Maximilian Herrmann, Jens Rauschenberger, Ronald Holzwarth, Hans A. Schuessler, Ferenc Krausz, and T W Hänsch, “A frequency comb in the extreme ultraviolet,” *Nature* **436**, 234–237 (2005).
- [55] Arman Cingöz, Dylan C. Yost, Thomas K. Allison, Axel Ruehl, Martin E. Fermann, Ingmar Hartl, and Jun Ye, “Direct frequency comb spectroscopy in the extreme ultraviolet,” *Nature* **482**, 68–71 (2012).
- [56] Stefano M. Cavaletto, Zoltán Harman, Christian Ott, Christian Buth, Thomas Pfeifer, and Christoph H. Keitel, “Broadband high-resolution X-ray frequency combs,” *Nature Photonics* **8**, 520–523 (2014).
- [57] Gil Porat, Christoph M. Heyl, Stephen B. Schoun, Craig Benko, Nadine Dörre, Kristan L. Corwin, and Jun Ye, “Phase-matched extreme-ultraviolet frequency-comb generation,” *Nature Photonics* **12**, 387–391 (2018).
- [58] KE Deitrick, GA Krafft, B Terzić, and JR Delaysen, “High-brilliance, high-flux compact inverse compton light source,” *Physical Review Accelerators and Beams* **21**, 080703 (2018).
- [59] Jan K Rudolph, S Bernitt, SW Epp, R Steinbrügge, C Beilmann, GV Brown, Sita Eberle, A Graf, Zoltan Harman, N Hell, *et al.*, “X-ray resonant photoexcitation: Linewidths and energies of k  $\alpha$  transitions in highly charged fe ions,” *Physical review letters* **111**, 103002 (2013).
- [60] Chunhai Lyu, Stefano M. Cavaletto, Christoph H. Keitel, and

- Zoltán Harman, “Interrogating the temporal coherence of euv frequency combs with highly charged ions,” *Phys. Rev. Lett.* **125**, 093201 (2020).
- [61] J. Nauta, J.-H. Oelmann, A. Borodin, A. Ackermann, P. Knauer, I. S. Muhammad, R. Pappenberger, T. Pfeifer, and J. R. Crespo López-Urrutia, “Xuv frequency comb production with an astigmatism-compensated enhancement cavity,” *Opt. Express* **29**, 2624–2636 (2021).
- [62] Inhyuk Nam, Chang-Ki Min, Bonggi Oh, Gyujin Kim, Donghyun Na, Young Jin Suh, Haeryong Yang, Myung Hoon Cho, Changbum Kim, Min-Jae Kim, *et al.*, “High-brightness self-seeded x-ray free-electron laser covering the 3.5 keV to 14.6 keV range,” *Nature Photonics*, 1–7 (2021).
- [63] Ichiro Inoue, Taito Osaka, Toru Hara, Takashi Tanaka, Takahiro Inagaki, Toru Fukui, Shunji Goto, Yuichi Inubushi, Hiroaki Kimura, Ryota Kinjo, *et al.*, “Generation of narrow-band x-ray free-electron laser via reflection self-seeding,” *Nature Photonics* **13**, 319–322 (2019).
- [64] E Allaria, D Castronovo, P Cinquegrana, P Craievich, Massimo Dal Forno, MB Danailov, G D’Auria, A Demidovich, G De Ninno, S Di Mitri, *et al.*, “Two-stage seeded soft-x-ray free-electron laser,” *Nature Photonics* **7**, 913–918 (2013).
- [65] S Dobosz, G Doumy, H Stabile, P D’oliveira, P Monot, F Réau, S Hüller, and Ph Martin, “Probing hot and dense laser-induced plasmas with ultrafast xuv pulses,” *Physical review letters* **95**, 025001 (2005).
- [66] Paul Gibbon, D Altenbernd, U Teubner, E Förster, Patrick Audebert, J-P Geindre, J-C Gauthier, and André Mysyrowicz, “Plasma density determination by transmission of laser-generated surface harmonics,” *Physical Review E* **55**, R6352 (1997).
- [67] W Theobald, R Hässner, C Wülker, and R Sauerbrey, “Temporally resolved measurement of electron densities ( $> 10^{23} \text{ cm}^{-3}$ ) with high harmonics,” *Physical review letters* **77**, 298 (1996).

## Supplemental Materials to the paper

### "High-brilliance ultra-narrow-band x-rays via electron radiation in colliding laser pulses"

Q. Z. Lv,<sup>1,\*</sup> E. Raicher,<sup>2,†</sup> C. H. Keitel,<sup>1</sup> and K. Z. Hatsagortsyan<sup>1</sup>

<sup>1</sup>Max-Planck-Institut für Kernphysik, Saupfercheckweg 1, 69117 Heidelberg, Germany

<sup>2</sup>Soreq Nuclear Research Center, 81800 Yavne, Israel

#### I. THE STRUCTURE OF THE HARMONICS

In this section, the details of the analytical estimations regarding the structure of harmonics, for example the harmonic width, the energy range of the x-ray comb and the optimized emitted angle, are presented. All the estimations are based on the analytical formula of the emission spectrum as well as the energy conservation law, which is well documented in our previous works [1, 2], and also verified by the numerical results in the main text.

The explicit formula for the radiation spectrum in general EM fields reads [3]:

$$dI = \frac{\alpha}{(2\pi)^2 \tau} \left[ -\frac{\varepsilon'^2 + \varepsilon^2}{2\varepsilon'^2} |\mathcal{T}_\mu|^2 + \frac{m^2 \omega^2}{2\varepsilon'^2 \varepsilon^2} |\mathcal{I}|^2 \right] d^3 \mathbf{k}', \quad (1)$$

where  $\mathcal{I} \equiv \int_{-\infty}^{\infty} e^{i\psi} dt$  and  $\mathcal{T}_\mu \equiv \int_{-\infty}^{\infty} v_\mu(t) e^{i\psi} dt$  with  $\psi \equiv \frac{\varepsilon}{\varepsilon'} k' \cdot x(t)$  being the emission phase and  $x_\mu, v_\mu, k'_\mu = (\omega', \mathbf{k}')$  are the four-vectors of the electron coordinate, the velocity and the photon momentum, respectively.  $\tau$  is the pulse duration. Since the oscillations in the energy is small in amplitude [1, 2], the average energy for the electron is  $\varepsilon$ , and  $\varepsilon' = \varepsilon - \omega'$ .

Let us first look at the phase  $\psi$  of the emission, which is a crucial parameter in the formalism and determines the structure of the harmonics of the spectrum,

$$\begin{aligned} \psi &= \frac{\varepsilon}{\varepsilon'} k' \cdot x(t) \\ &= \psi_{np} t - z_2 \sin(\omega_2 t) - z_1 \sin(\omega_1 t) - z_3 \sin(\Delta\omega_{12} t). \end{aligned} \quad (2)$$

Introducing the definition of  $u = \omega'/\varepsilon'$ ,  $\omega_1 = (1 + v_z)\omega_0 \approx 2\omega_0$ ,  $\omega_2 = (1 - v_z)\omega_0 \approx \omega_0/2\gamma_*^2$  and  $\Delta\omega_{12} = \omega_2 - \omega_1$  with  $v_z$  being the average velocity on axis and  $\gamma_* = \varepsilon/m_*$  where the effective mass  $m_* \equiv m \sqrt{1 + \xi_1^2 + \xi_2^2}$ , we may write

$$\begin{aligned} \psi_{np} &\equiv \varepsilon u (1 - v_z \cos \theta), \quad z_1 \equiv \frac{m u \xi_1}{\omega_1} \sin \theta, \\ z_2 &\equiv \frac{m u \xi_2}{\omega_2} \sin \theta, \quad z_3 \equiv \frac{2\omega_0 m^2 u \xi_1 \xi_2}{\varepsilon \Delta\omega_{12}^2} \cos \theta. \end{aligned} \quad (3)$$

With the analytical solution of the time integral in Eq. (1), one obtains

$$\mathcal{T}_\mu = 2\pi \sum_{s_1} \sum_{s_2} \mathcal{M}_\mu(s_1, s_2, \omega', \cos \theta) \delta(\Omega_{s_1, s_2}), \quad (4)$$

\* qingzheng.lyu@mpi-hd.mpg.de

† erez.raicher@mail.huji.ac.il

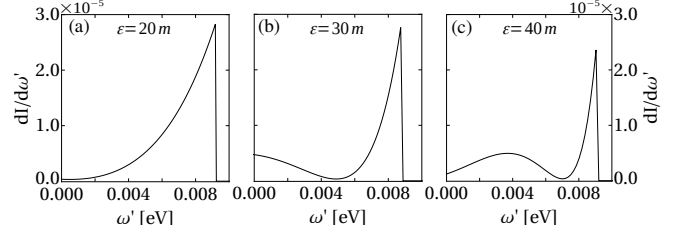


Figure S1. The spectra according to the analytical expressions of Eq. (1) for  $\xi_1 = 0.1$  and  $\xi_2 = 2$  with different energies. In order to show the narrow width of the peaks, the x-axis has been shifted to the right by 494.928 eV for (a), by 1103.835 eV for (b) and by 1982.290 eV for (c). Here the spectra are calculated by the analytical formulas in Ref. [2].

where  $s_1$  and  $s_2$  denote the absorbed photon number from  $\xi_1$  and  $\xi_2$  pulse, respectively. The matrix elements can be expressed as the multiplication of Bessel functions with arguments  $z_1, z_2, z_3$  [2]. Furthermore, based on the argument of the  $\delta$ -function, the energy conservation can be written as

$$\begin{aligned} \omega' &= \frac{\varepsilon(s_1 \omega_1 + s_2 \omega_2)}{\varepsilon(1 - v_z \cos \theta) + (s_1 \omega_1 + s_2 \omega_2)} \\ &\approx \frac{2\gamma_*^2 (s_1 \omega_1 + s_2 \omega_2)}{1 + 2\gamma_*^2 (1 - \cos \theta)}. \end{aligned} \quad (5)$$

The last step involves the approximation connected with the neglect of the recoil as  $\chi \ll 1$ . The emission is nearly on axis ( $\theta \sim 0$ ) and can thus be confined to a small range  $0 < \theta < \theta_w$ . The width of the harmonic due to this finite angle window is  $\delta\omega'_w = \omega'(\theta = 0) - \omega'(\theta = \theta_w)$ . Employing Eq. (5) and Taylor expanding for  $\theta \ll 1$  one obtains

$$\delta\omega'_w = \omega_{s_1, s_2}^m (\gamma_* \theta_w)^2. \quad (6)$$

where  $\omega_{s_1, s_2}^m = 2\gamma_*^2 (s_1 \omega_1 + s_2 \omega_2)$ .

As seen from the main text, the harmonics we are interested in are determined by the  $\xi_2$ -laser co-propagating with the electrons. The structure of the harmonics are therefore related with  $z_2$  and the corresponding Bessel functions as well as the emission angle  $\theta$ . According to Eq. (5), the corresponding sine function is approximately given by  $\sin \theta \approx \sqrt{1 - 1/v_z^2 + 2(s_1 \omega_1 + s_2 \omega_2)/(\varepsilon u v_z^2)}$ . Substituting this expression into Eq. (3) one obtains

$$z_2 = \frac{\xi_2 m_* m}{\omega_2 \varepsilon} \sqrt{u(u_s - u)}, \quad (7)$$

where  $u_s \equiv 2\varepsilon(s_1 \omega_1 + s_2 \omega_2)/m_*^2$ . The main harmonics in Fig. 3 of the paper correspond to  $s_1 = 1$  and  $s_2 \sim 1$ , which



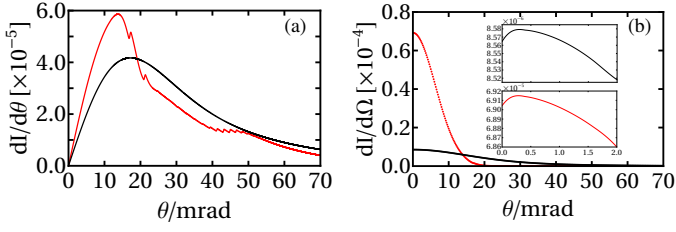


Figure S2. The angle-resolved radiation intensity for CS (black) and Case I of CPW (red): (a) Intensity per emission angle  $dI/d\theta$ ; (b) Intensity per solid angle  $dI/d\Omega$ . The insets in (a) and (b) show  $dI/d\theta$  for small  $\theta$ . All other parameters are the same as Fig. 2 in the paper.

means  $u_s \approx 2\varepsilon\omega_1/m_*^2$ . Then, the width  $\delta u$  can be estimated according to  $z_2 \approx s_2$  in this regime and expressed as

$$\delta u = \frac{\omega_2^2 \varepsilon}{2\xi_2^2 \omega_1 m^2}. \quad (8)$$

Therefore, according to  $u = \omega'/\varepsilon'$ , the intrinsic width of the peak  $\delta\omega'_c$  is approximately

$$\delta\omega'_c = \frac{\varepsilon^2 \omega_2^2}{2\xi_2^2 \omega_1 m^2 + \varepsilon \omega_2^2} \approx \frac{\omega_2}{8} \left( \frac{m_*}{m\xi_2} \right)^2. \quad (9)$$

In the last step, we have neglected the photon recoil for simplicity. From this estimation, we can see that the width is decreasing with the increasing of the electron energy, seen in Fig. S1. According to Eq. (9), the full width at half maximum of the peak is 0.00313eV for panel (a), 0.00138eV for panel (b) and 0.00076eV for panel (c), which is approximately proportional to  $1/\gamma_*^2$ . This is in contrast with the width of the harmonic in the single plane wave case, where  $\delta\omega' \sim \omega_0 \gamma^2 / \xi^2$  increases with the electron energy.

Meanwhile, we can also estimate the optimized emitted angle of the photons. Since the emission in our setup is almost on axis, the Bessel function argument in Eq. (3) can thus be rewritten as  $z_2 \approx m\xi_2 u / \omega_2$ . As the main peak appears when  $u = u_s \approx 2\varepsilon\omega_1/m_*^2$  and  $z_2 \sim 1$ , the optimized angle  $\theta_{op}$  is

$$\theta_{op} = \frac{m_*^2}{8\gamma\xi_2^2\varepsilon^2}, \quad (10)$$

which also decreases with the electron energy. This coincides with Fig. 4(b) in the main text. It is also worth to point out that this optimized angle is different from the scattering of an electron from a circularly polarized plane wave laser pulse with the optimized emitted angle around  $\xi_1/\gamma$ .

From  $z_2 \approx m\xi_2 u / \omega_2$ , we can also see that  $z_2$  tends to 1 for the angle  $\theta \sim 0$  as  $\omega_2$  being rather small. This explains the almost on axis emission in the CPW setup. In the opposite, the harmonics in common CS, which triggered by  $\xi_1$  only, is determined by  $z_1$  and thus the harmonics center for larger angles according to Eq. (3).

Another interesting property of the spectrum is the energy range of the x-ray comb for the case of  $\xi_2 > \xi_1$ . As explained

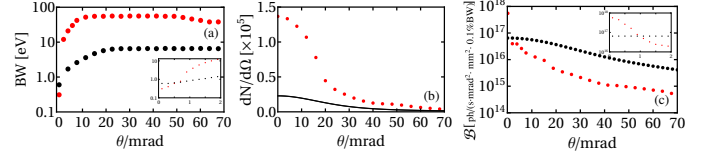


Figure S3. (a) The bandwidth (BW) of the spectrum as a function of angle  $\theta$  for CS (black dots) and for Case I of CPW setup (red dots); (b) The photon number  $dN/d\Omega$  as a function of angle  $\theta$  for CS (black dots) and for Case I of CPW setup (red dots). The insets in (a) and (c) show the BW and brilliance for small  $\theta$ . Here the angle window is kept to be 0.2mrad for all  $\theta$  in the calculations. All the other parameters are the same as Fig. 2 in the paper.

in the paper, the peaks are equally distant with the laser basic frequency  $\omega_0$ , the estimation of this range is equivalent to estimating the number of peaks in the comb-like structure. The peaks are determined by Bessel functions with the argument of  $z_2$ , the same as for the intrinsic width. It is well known that a Bessel function tends to be zero when the argument is much smaller than the order of the function. Therefore, the peak appears only when  $z_2/\Delta s_2 = \delta \sim 1$ . With a given emitted angle window  $0 < \theta < \theta_w$  as before,  $z_2$  can be approximated as  $2\xi_2\theta_w\varepsilon(\Delta s_2\omega_2 + \omega_1)/(\omega_2 m_*^2)$ . Therefore, we can solve for  $\Delta s_2$  based on  $z_2 = \delta\Delta s_2$  and obtain

$$\Delta s_2 = \frac{2\xi_2\varepsilon\omega_1\theta_w}{\delta\omega_2 m_*^2 + 2\xi_2\varepsilon\omega_2\theta_w} \approx \frac{1}{\delta} \left( \frac{\theta_w}{\theta_c} \right). \quad (11)$$

with  $\theta_c = m_*/(8m\xi_2\gamma_*^3)$  according to  $\delta\omega'_w(\theta_c) = \delta\omega'_c$ . From this formula we can see that the number of peaks is proportional to the angle spreading  $\theta_w$  of the radiation. If we choose the optimized angle in Eq. (10),  $\Delta s_2$  is proportional to  $1/\xi_2$ , which means that by lowering the strength of the  $\xi_2$ -laser in the CPW configuration, the range of the comb-like structure can be extended.

## II. DETAILED COMPARISON OF COMMON COMPTON SCATTERING WITH THE COUNTER-PROPAGATING WAVE SETUP

Let us clarify at which emission angle the brilliance is largest for CS with the laser and electron parameters used in the paper. From Fig. 1 in the main text, we can see that the general form of the spectra for all cases is the same as it is determined by  $\xi_1$  laser and therefore the main radiation in Case I and II for the CPW setup is similar like in the CS case that distributes in a large angle range. We confined the emitted angle in a small range in order to achieve an extreme narrow BW. For the range of  $\theta < 0.2$  mrad in Case I, the emitted energy is only  $4.7 \times 10^{-5}$  of the total energy in all directions and this ratio becomes  $1.2 \times 10^{-3}$  for  $\theta < 1.0$  mrad. This low relative portion is the price to pay in order to obtain monochromatic radiation and our scheme is more favorable for applications which require ultra-narrow band sources.

In our calculations for normal CS and Case I of CPW setup,

the counter-propagating laser  $\xi_1 = 0.1$ , and therefore, the emission will be within the  $1/\gamma$ -cone. From Fig. S2, we can see that the intensity in a unit solid angle  $dI/d\Omega$  for both CS and Case I is largest in the forward direction and decreases monotonically with increasing  $\theta$ . The emission for Case I is more concentrated in the forward direction because of the co-propagating laser pulse ( $\xi_2$ ), but the total emission energy is similar for both CS and Case I as demonstrated in Fig. 1(c-e) of the paper.

The radiation BW for both CS and Case I is shown in Fig. S3. For small  $\theta$  the BW for Case I is smaller than that for CS. However, the BW for Case I increases rapidly, when  $\theta$  is increasing and then reaches a constant for large  $\theta$ . This is because different harmonics of the  $\xi_2$  laser overlap with each other for large  $\theta$ , and the BW in this case is determined only by the angle window, see the angle resolved spectrum in Fig. 2 of the paper. The angle dependence of the emitted photon number and brilliance are shown Fig. S3 (b) and (c). The brilliance decreases with  $\theta$  for both cases. At large angles brilliance of CS is larger than for CPW Case I. However, in the forward direction Case I shows larger brilliance with respect to CS, see inset in Fig. S3 (c). This advantage comes from the small BW and large photon number in the forward direction. Therefore, to show the advantage of our CPW scheme in brilliance with respect to CS, we will carry out a comparison at  $\theta = 0$ .

In CS and the discussed CPW scheme the radiation is distributed in a rather large angle and frequency region, with a frequency-angle relationship according to the energy-momentum conservation [Eq.(2) of the paper]. To have a narrow bandwidth radiation, one needs to restrict the emission angle. In both cases, CS and CPW, the most beneficial for a small emission BW is the region near forward direction ( $\theta = 0$ ), when  $\partial\omega'/\partial\theta = 0$ , see Fig. 2(a,d) of the paper. Then, when applying a rather small angle window  $\Delta\theta_w$ , the BW becomes not dependent on the window, but is determined by the dynamical linewidth. At a given small angular window, the dynamical BW for CPW is significantly narrower than in CS, which is due to the properties of the spectral spikes in CPW. In the CPW setup new satellite peaks arise with  $\omega_0$  separation, and the smooth energy distribution within a large BW for CS, roams into these sharp spikes. The Figs. 2(b,e) of the paper show a comparison of the emission in CS with that of the CPW Case I. Using the same angle window  $\Delta\theta_w = 0.2$  mrad around  $\theta = 0$ , the relative BW in CS for a single electron is  $\Delta\omega'/\omega' \approx 10^{-4}$ , while in the CPW Case I it is 2 times smaller due to the smallness of the dynamical BW, see zoom in Figs. 2(g,h) of the paper (dashed lines are for a monochromatic electron beam). However, the number of photons in the line in the CPW case is about 7 times larger than in CS, which is due to more prominent forward emission in CPW, see Fig. S2 (b).

This can also be seen from the angular distributions of the radiation intensity for different harmonics in all cases as shown in Fig. S4. For CS [Panel (a)], we choose  $s_1 = 1$ , as at  $\xi_1 = 0.1$  other harmonics are suppressed. For CPW Case I [Panel (b)] with  $s_1 = 1$ , the distribution is oscillating and the emitted energy for small angles is certainly larger than for common CS in Panel (a). By varying  $s_2$ , we can see that for different harmonics the emission is centered in different angle regions, which produces a single peak spectrum if we confine the angle

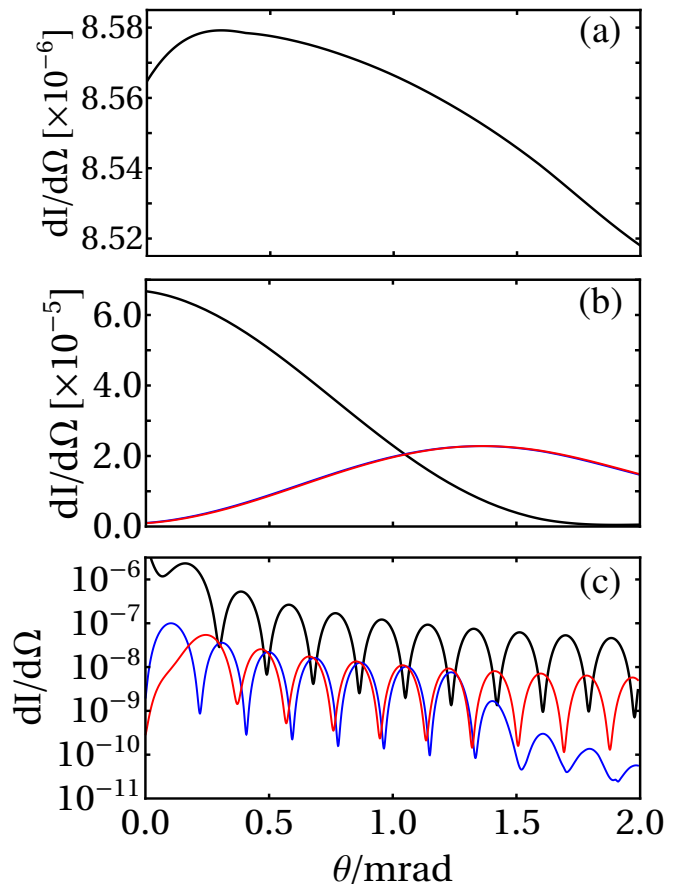


Figure S4. The angular distribution of radiation intensity: (a) CS; (b) CPW Case I; (c) CPW Case II. In all the cases,  $s_1 = 1$ ,  $s_2 = -1$  (blue curve),  $s_2 = 0$  (black curve) and  $s_2 = 1$  (red curve), for both CPW Case I and Case II. The parameters are the same as in Fig. 2 in the paper.

range. For Case II [Panel (c)], there are more oscillating in the same angle range for different harmonics and therefore it produces a comb structure in the frequency domain.

Due to these properties of the radiation, the brilliance for Case I in CPW is higher than that for CS. For a monochromatic electron beam the brilliance enhancement is approximately 14 ( $7 \times 2$ ) times. In the paper we have considered also the case of a realistic electron beam with an energy spread and emittance. We use the electron beam with the energy spread of the order of  $\Delta\gamma/\gamma \sim 10^{-4}$  and an angular spread of the order of  $\Delta\theta \sim 10^{-3}$ , which is envisaged in [4]. In this case BW for CS is 1.4 times larger than for CPW, see Figs. 2(g,h) of the paper, leaving however, the number of photons in the emission line equal to the case without spreading. Thus, we can have an order of magnitude larger brilliance in the CPW Case I with respect to CS with the same laser and electron parameters. For instance using an electron beam with 10pC charge and 0.1% angle spreading (emittance of 0.1 mm-mrad) and 0.01% energy spreading at electron energy  $\varepsilon = 10$  MeV, the peak brilliance in forward direction for CPW Case I is  $\mathcal{B} \sim 5.2 \times 10^{18}$

ph/(s·mrad<sup>2</sup>·mm<sup>2</sup>·0.1%BW), while in the corresponding CS it is  $\mathcal{B} \sim 6.5 \times 10^{17}$  ph/(s·mrad<sup>2</sup>·mm<sup>2</sup>·0.1%BW).

In order to obtain the largest brilliance for a realistic electron beam with a duration of  $T_e$ , each electron in the beam has to overlap with both of the laser pulses during interaction. The duration of the overlap of the electron beam with counter-propagating laser pulse is  $\tau_1 \approx (T_1 - T_e)/2$  with  $T_i = N_i T_L$  and the laser period  $T_L$ , which is also the total duration of the electron beam emission. During this time each electron should experience at least 5 cycles of the co-propagating laser beam:  $(c - v)\tau_1 > 5cT_L$ , i.e.

$$T_1 - T_e > 20\gamma_*^2 T_L. \quad (12)$$

All electrons in the beam should experience the co-propagating laser pulse, therefore, the electron beam should overlap with  $\xi_2$  from the beginning of the interaction to the end and the length of the  $\xi_2$ -pulse should be longer than the electron beam, such that  $c(T_2 - T_e)/(c - v) = \tau_1$ . From the latter we derive the condition:

$$T_2 - T_e > \frac{T_1}{4\gamma_*^2}. \quad (13)$$

For the applied parameters in Case I,  $\gamma_* \approx 20$ ,  $T_1 = 16000T_L$ , and from Eq. (12), we have  $T_e < 8000T_L = 20$  ps;  $T_1/(4\gamma_*^2) \sim 10T_L$ , i.e., practically  $T_2 \gtrsim T_e$ . We choose  $T_2 \approx T_e = 2$  ps and this choice is feasible as  $\xi_2 \ll 1$ . For Case II where  $\xi_2 \sim 1$ , the pulse length or the transverse radius for the  $\xi_2$  laser has to be smaller than the electron beam so that the laser can still be table-top size. This will decrease the brilliance but the comb structure in hard x-ray regime can be preserved. Hence, our scheme is feasible to operate with electron beams of a picosecond duration provided by usual electron accelerators, and using co-propagating long laser pulses of a picosecond duration. Note that the emitted x-ray pulse duration is  $\tau_x = \tau_1(c - v)/c + T_e \approx (T_1 - T_e)/(4\gamma_*^2) + T_e \approx T_e$ , which is taken into account in the estimation of brilliance.

### III. THE SPECTRA FOR VARIOUS ENERGY AND ANGLE WINDOWS IN THE CPW SETUP

As discussed in the main text, the BW of the spectrum in the CPW setup is determined by three different factors. In Fig. S5, we show the interplay between different electron energies and emitted angle ranges. In case I,  $m_*/(m\xi_2) \gg 1$ , the dynamical BW  $\delta\omega'_{in} \approx \omega'_0$  is of the same order as the spacing  $\Delta\omega' = \omega_0$  between peaks. Hence, enlarging  $\delta\omega'_w$  results in gradually widening the peak. A different behaviour is seen for case II [lower panel], when  $\delta\omega'_{in} \approx \delta\omega'_f \ll \omega_0$ . Since  $\delta\omega'_f$  does not depend on the energy and angle, the BW in case II originates from  $\delta\omega'_w \sim \gamma^2$ , which surpasses  $\delta\omega'_{in}$  at  $\varepsilon \gtrsim 30m$ . For both cases in Fig. S5 the relative BW of the harmonics in the spectra can be as small as  $10^{-4}$  for both case I and case II, which is similar compared with that of XFEL.

In order to have a comprehensive picture of the impact of the electron energy and the emitted angle on the structure of the harmonics, we present the signal to noise ratio,  $R_{SN} = I_{max}/I_{min}$ ,

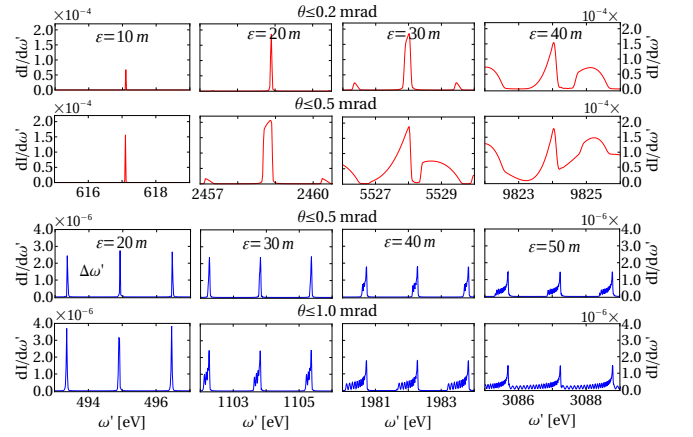


Figure S5. The spectral line's BW for different electron energies and different angle ranges: (upper panel, red curves) case I with  $\xi_1 = 0.1$  and  $\xi_2 = 0.02$ ; (lower panel, blue curves) case II with  $\xi_1 = 0.1$  and  $\xi_2 = 2$ . The pulse length for  $\xi_1$  is  $N_1 = 80000$ .

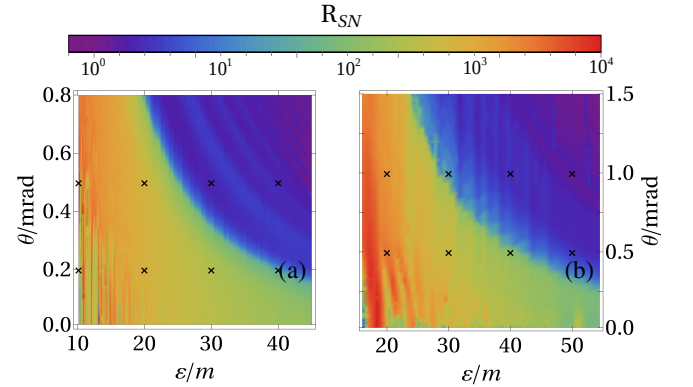


Figure S6. The signal-to-noise ratio  $R_{SN}$  vs  $\varepsilon$  and  $\theta$ : (a) for  $\xi_1 = 0.1$  and  $\xi_2 = 0.02$  and (b) for  $\xi_1 = 0.1$  and  $\xi_2 = 2$ . The pulse length for  $\xi_1$  is  $N_1 = 80000$  for both cases. The oscillations in the plot stem from the background emission which induces oscillations in  $I_{min}$ , especially for case II. The crosses show the parameters considered in Fig. S5.

for the two cases in Fig. S6(a) and (b). Here  $I_{max}$  is the intensity at the main peak, while  $I_{min}$  is the intensity at the middle point between the main peak and the adjacent one. By scanning over both  $\varepsilon$  and  $\theta$ , we can see that the larger the electron energy, the smaller the angle should be such that the isolated peaks are sharp enough ( $R_{SN} > 100$ ). The sudden jump in  $R_{SN}$  for both cases corresponds to the situation where the angle width reaches the middle point,  $\delta\omega'_w = \omega_0/2$ .

### IV. THE APPLICATION OF THE COMB-LIKE STRUCTURE IN THE X-RAY REGIME

The comb-like structure in the hard x-ray regime can be obtained by changing the intensity of the two lasers in the CPW setup. Compared with the comb in the EUV regime, the

most energetic frequency comb available in the lab now, the comb-like structure in the x-ray regime is a completely new experimental tool and can find applications in different fields. For example, it may be applied to probe ultra-dense plasma samples in a wide range of regimes such as inertial confinement fusion, laser-plasma interaction, as well as laboratory astrophysics. The free electron density and the temperature of a dense plasma can be determined by measuring the absolute transmission of two harmonics from high-order harmonics generated in a gas jet, see Refs [5–7]. The frequency comb described in this work enables probing plasma samples with much higher density as it lies in the x-ray domain. In addition, it dramatically improves the accuracy of the measurement since the single peak in the comb is ultra narrow and the relative spacing between two peaks is much smaller compared with

radiation sources based on high-order harmonics generation. Moreover, the large frequency range of the comb allows for measuring a large density regime in a single shot. Secondly, the comb-structure can also be used in probing highly charged ion systems. Recent experiments, see Ref [8], on determining the transitions in highly charged iron ions scanned over a large energy region employing a monochromatic x-ray laser pulse from XFEL facility. It is realized by applying a crystal monochromator. However, the frequency range of the monochromator is fixed by its crystal properties, and cannot be modified. On the contrary, the energy of the frequency comb proposed here may be freely tuned. Furthermore, by utilizing the comb, one can probe a much larger energy range in a single shot. On the other hand, because the electron energy and the laser intensity needed are rather moderate, this setup is of table-top size, relatively affordable and anticipated easy to operate.

- 
- [1] Q. Z. Lv, E. Raicher, C. H. Keitel, and K. Z. Hatsagortsyan, “Anomalous violation of the local constant field approximation in colliding laser beams,” *Physical Review Research* **3**, 013214 (2021).
- [2] Q Z Lv, E Raicher, C H Keitel, and K Z Hatsagortsyan, “Ultra-relativistic electrons in counterpropagating laser beams,” *New Journal of Physics* **23**, 065005 (2021).
- [3] V. N. Baier, V. M. Katkov, and V. M. Strakhovenko, *Electromagnetic Processes at High Energies in Oriented Single Crystals* (World Scientific, Singapore, 1994).
- [4] KE Deitrick, GA Krafft, B Terzić, and JR Delayen, “High-brilliance, high-flux compact inverse compton light source,” *Physical Review Accelerators and Beams* **21**, 080703 (2018).
- [5] S Dobosz, G Doumy, H Stabile, P D’oliveira, P Monot, F Réau, S Hüller, and Ph Martin, “Probing hot and dense laser-induced plasmas with ultrafast xuv pulses,” *Physical review letters* **95**, 025001 (2005).
- [6] Paul Gibbon, D Altenbernd, U Teubner, E Förster, Patrick Audebert, J-P Geindre, J-C Gauthier, and André Mysyrowicz, “Plasma density determination by transmission of laser-generated surface harmonics,” *Physical Review E* **55**, R6352 (1997).
- [7] W Theobald, R Hässner, C Wülker, and R Sauerbrey, “Temporally resolved measurement of electron densities ( $> 10^{23} \text{ cm}^{-3}$ ) with high harmonics,” *Physical review letters* **77**, 298 (1996).
- [8] Jan K Rudolph, S Bernitt, SW Epp, R Steinbrügge, C Beilmann, GV Brown, Sita Eberle, A Graf, Zoltan Harman, N Hell, *et al.*, “X-ray resonant photoexcitation: Linewidths and energies of  $k \alpha$  transitions in highly charged Fe ions,” *Physical review letters* **111**, 103002 (2013).